Understanding MilliQan: An Analysis of Position-Based Effects

Lukas Kiekover
Department of Physics, Montana State University

David Stuart (Faculty Advisor) and Dariush Imani (Graduate Advisor)
Department of Physics, University of California, Santa Barbara
(Dated: October 2, 2025)

We introduce the milliQan experiment as a search for millicharged particles produced at the Large Hadron Collider (LHC). We then examine data taken on a similarly constructed detector using cosmic ray scans to uncover position-based effects. These scans reveal the existence of a "cutoff angle", where the sensitivity of the detector suddenly falls off. We also develop a simulation to study PMT light collection efficiency as a function of the position and angle of a cosmic ray as it enters the scintillator. This simulation allows for direct comparison with real data, which in turn allows us to validate our understanding of position-based effects, like the cutoff angle, on the sensitivity of the milliQan slab detector.

I. INTRODUCTION

The Standard Model (SM) is one of the fundamental cornerstones of modern particle physics. It defines for us many of the phenomena we see, and it has correctly predicted a number of particles and properties since its introduction. However, the SM is not perfect. It lacks descriptions of some known phenomena and has been found to be incorrect in its description of others. For example, the SM does not describe gravity, and it predicted that neutrinos were massless, which was later proven false. It also lacks a description for something called dark matter, which is matter that interacts very feebly, if at all, with photons, and it is extremely hard to characterize because of that. Dark matter does, however, interact via gravity, and through observing those interactions, it has been estimated to compose about 85% of all matter in the universe.[1, 2]

Many models have been developed that propose dark matter candidates which often also serve as explanations for oddities found in SM physics. For example, weakly interacting massive particles (WIMPs) have been proposed as a dark matter candidate and also happen to be useful for satisfying supersymmetry (SUSY) theories.[3] Similarly, a predicted symmetry breaking in the strong interaction has led to the proposal of a new boson called an axion.[4] These candidates, in particular WIMPs, have been searched for extensively, but no definitive evidence that support these models has been found.[5, 6] This has motivated physicists into exploring a different set of models which instead propose a "dark sector" (DS) which contains not just new dark matter candidates, but also a new set of interactions that govern these particles.

These DS models are all predicated on the idea that there exists some kind of "portal" where there is coupling between SM and DS physics, as illustrated in Figure 1.[7] One model that has grown more prevalent over the last decade is the "dark photon portal". This model predicts a feeble coupling of the photon and a "dark photon" which governs a DS interaction. This model has become more prevalent in particular because a predicted effect of the coupling is the generation of particles with a suppressed electric charge on the order of $e \times 10^{-3}$, so-called "millicharged particles" (mCPs).[8] If one could find these mCPs, it would strongly suggest the existence of this dark photon.

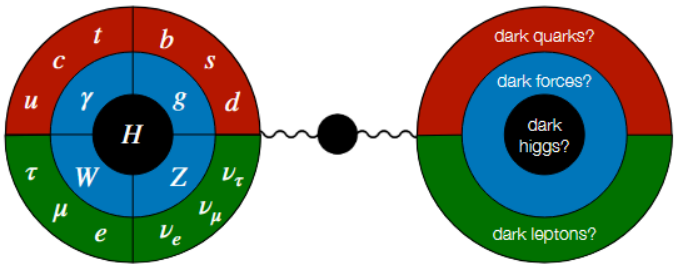

FIG. 1. Cartoon displaying relationship between the Standard Model and dark sector via a portal. The dark sector may contain the same complexity observed in ordinary matter.

The real challenge with that, though, is that mCPs interact so feebly that they require dedicated detectors. Although many searches have been conducted in the past, there are still many regions of the charge-mass parameter space that remain unexplored. MilliQan aims to probe one of those regions, as seen in Figure 2, by placing two specialized detectors in a drainage gallery near the CMS experiment at CERN.[9]

A. MilliQan

MilliQan is sited at LHC Point 5 in the PX56 drainage gallery, 33 m from the CMS experiment. 17 m of that length is solid rock, providing shielding from much of the unwanted radiation and particles generated by the collisions of the CMS experiment. MilliQan consists of two

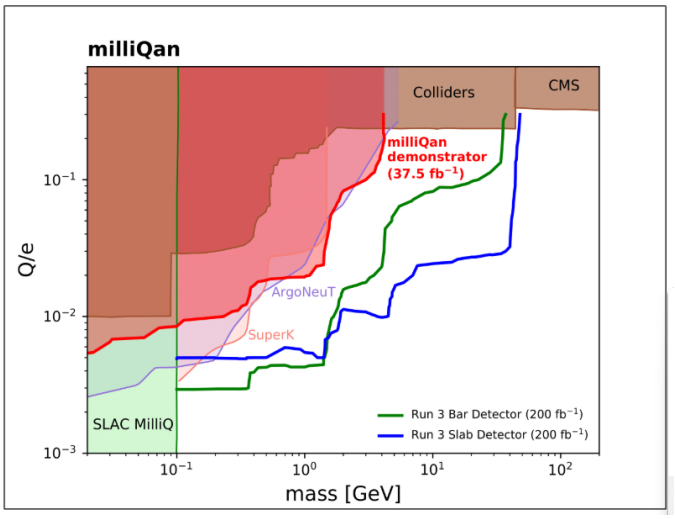

FIG. 2. Graph of parameter space where mCPs may exist, milliQan will cover the area above the blue and green lines.

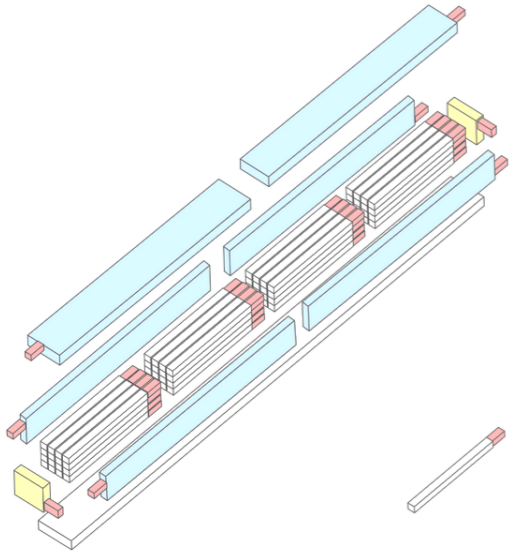

FIG. 3. Model of the bar detector

detectors composed of plastic scintillators in tandem with photomultiplier tubes (PMTs)[10, 11]. As a charged particle passes through the scintillators, a number of photons are produced proportional to the energy deposition of the particle, which itself is proportional to Q^2. The PMTs operate using the photo-electric effect. A photon is absorbed by the photocathode, resulting in the emission of a photoelectron. The photoelectron is then accelerated into a series of dynodes designed to release more and more electrons upon each impact. This cascade of electrons then collides with an anode, where it is converted into an electric pulse that can be read. In tandem, the scintillators and PMTs effectively convert the charge of a particle to pulses of a certain shape and size, which we can analyze. The experiment is designed to probe charges from $10^{-3} \lesssim \frac{Q}{e} \lesssim 10^{-1}$ on masses ranging from 10^{-1} GeV to 100 GeV.[9] However, this area cannot practically be covered by a single detector, so instead, we use two separate geometries, dubbed the "bar" and "slab" detectors.

The bar detector, seen in Figure 3, serves to cover a larger charge range in this experiment. It consists of four layers of 4 bar $\times$ 4 bar arrays, making 64 bars total. Each bar is a long, narrow rectangular scintillator with one PMT on the end. This detector covers more of the lower charge range by maximizing the distance traveled by any particle passing through the detector, allowing for a larger energy deposition and the production of more photons. This decreases the possibility of an mCP traveling through the detector and simply not producing enough photons to create a response.

The slab detector serves to cover a larger mass range than the bar detector by casting a larger net. It is constructed using larger scintillator slabs, each having four PMTs. These slabs are set up in arrays stacked on top of each other with spacings between them, as seen in Figure 4. The layers are set up to match the approximate angle of an incoming particle from the CMS experiment. This setup is significantly less efficient at detecting lower-charge mCPs, however it is much more likely to catch more of the larger mass particles simply by covering a larger solid angle.

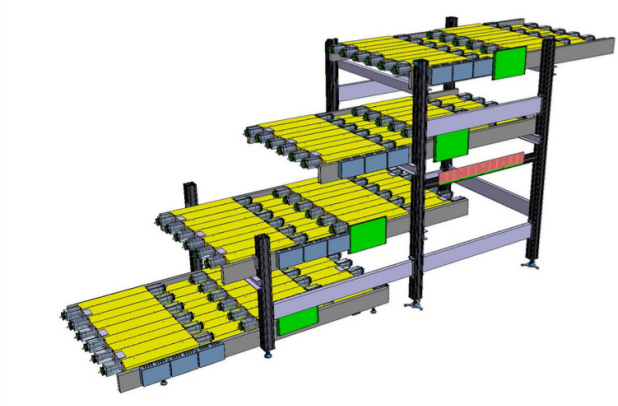

FIG. 4. Model of the slab detector.

Because of its narrow geometry, the bar detector is only weakly affected by the angle and position of incoming particles. In contrast, the wide geometry of the slab detector makes these factors strongly influence the travel path of the photons they produce. This, in turn, determines whether the photons can reach the PMTs and generate a pulse, making the photon collection efficiency strongly dependent on where and at what angle a particle enters the scintillators. Understanding these position-based effects, therefore, is extremely important to understanding the detector's overall sensitivity.

II. SLAB ANALYSIS AT UCSB

To gain an understanding of these position-based effects, we analyzed the cosmic ray response of a similar detector located in our lab. To do this we made an adjustable setup consisting of two single bars from the bar detector and a large slab scintillator. These bar detectors are laid one on top of the other, perpendicular to each other, making a plus-sign that is laid on the slab, aligned with its walls. There are four PMTs used in this setup: one at the end of either bar, and two in line with each other on opposite sides of the slab. The PMTs on the slab will be referred to as CH3 and CH4. For any reading we get from this setup, we require a response from all four PMTs almost simultaneously. This effectively requires that a cosmic ray travels through the small area where the two bars overlap and that we get data from both slab PMTs. We can adjust this setup by moving the bars to various positions on the slab, allowing us to measure the response from a cosmic ray that travels through any area we choose on the slab. With this, we can see how the response changes based on the position of the bars and identify trends.

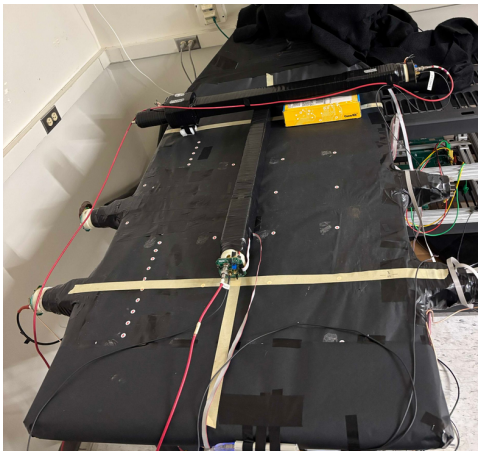

FIG. 5. The setup used in our experiment. To avoid light leaks, we also covered the detectors with a large felt cover.

We started by taking scans across much of the length of the slab, centered between the two PMTs, then across the width of the slab, along the line between the two PMTs. These scans were followed by a series of scattered measurements motivated by various phenomena seen in the raw data. The pulses recorded in these scans are automatically sent into a database and processed into a series of neat plots and histograms. The histograms we found most relevant to this project displayed the pulse area of each trigger as seen in Figure 6. These histograms typically take the form of Landau distributions. We record the most probable value (MPV) of the peaks of these landaus, as it is an effective representation of relative light collection efficiency. The uncertainty in these values is dependent on the width and general quality of the

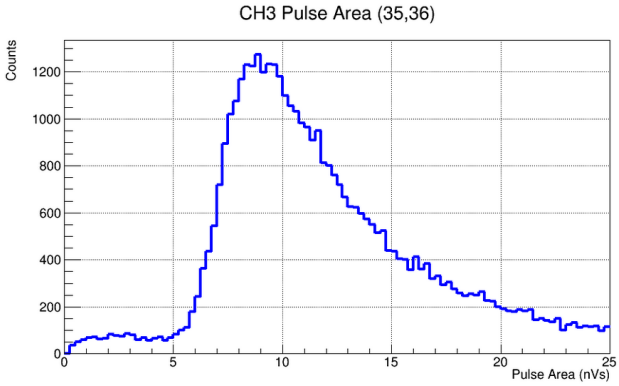

FIG. 6. Histogram of pulse area seen in the CH3 PMT 35 cm down the length of the slab and 36 cm along its width.

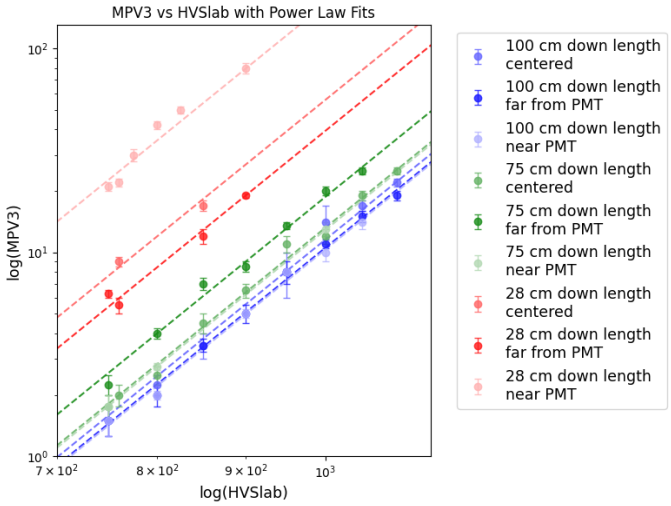

FIG. 7. Plot of a series of power law fits applied to points across the slab.

landau. We see it typically in the range of 5% to 10% uncertainty.

There are more factors than just position governing the MPVs, namely the powering high voltage (HV) for the slab PMTs. Fortunately, the PMT gain scales with the applied HV via a power law. To confirm this, multiple runs were taken at nine positions, each with varying HV. The MPVs and HV were recorded and applied to a series of power law fits, with the added requirement that the parameter corresponding to the slope of the fits seen in Figure 7 is shared between all positions. This parameter is known to be solely dependent on the electronics in the PMTs, and due to that parameter being well established and constant, previous and future scans consisting of only one HV per position could be fitted as well. These fits are then extrapolated out to the HV of the milliQan slab detector, 1450 V, and the MPV at that point is recorded. These new extrapolated MPVs are now effectively dependent solely on the varying position, and can be used as a calibrated dataset for subsequent analysis.

III. POSITION BASED EFFECTS

To begin analyzing this calibrated, we first made a 2D histogram of the MPVs for CH3. We also interpolated between points using polynomial methods to create Figure 8, an effective map of CH3 light collection. A similar map is made for CH4 to confirm relative symmetry. These maps present us with a good visualization of many of the obvious features that we had been expecting, namely that the collection efficiency is reduced further away from the PMT. Another feature that was predicted and is quite visible in this map is an angular dependence, more aptly the existence of a "cutoff angle", where positions beyond an angle relative to the normal of the PMT have a sudden drop in light collection efficiency.

To confirm the existence of this cutoff angle, we calculated the angle between the center point of the measured areas and the normal to the center of the PMT. We then plotted the extrapolated MPV value against those angles for various positions, resulting in Figure 9. Two facts became clear in the analysis of these plots. First, the cutoff angle is located at approximately 40°. Second, the steepness of that cutoff is distance dependent, decreasing further away from the PMT.

An complicating effect of selecting an area on the slab and the reduction we see in cutoff severity is that we lack the resolution to do any more than locate an approximate cutoff angle. Near the PMT, the runs would have to be taken so close to one another that randomness in where cosmic rays hit our selected area would smear the angle and provide too much uncertainty to precisely determine the value. Further from the PMT, the effect is simply too weak to confidently differentiate any cutoff from uncertainty. However, the specific value for the cutoff angle is largely unimportant here. The cutoff effect could result from a number of factors, including, but not limited to, surface roughness, total internal reflection, and the PMTs own angular dependence. It is quite likely that the exact angle will vary slightly between this detector and the milliQan slab detector. Simply knowing that the effect exists at this approximate angle proide a basis to develop information to develop a better understanding of the light collection of the milliQan slab detector.

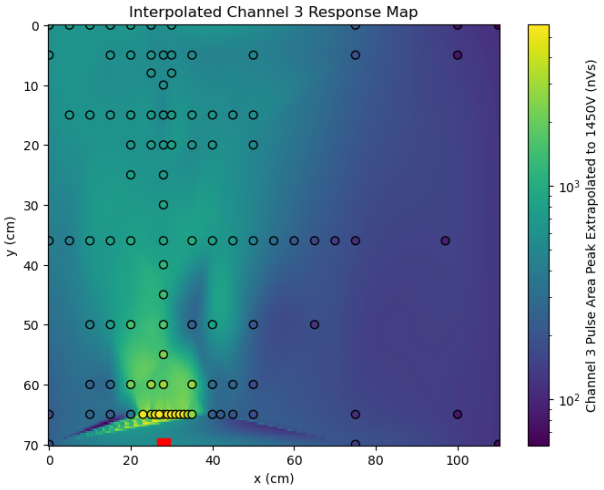

FIG. 8. An interpolated 2D histogram containing the CH3 response for every point tested on the slab.

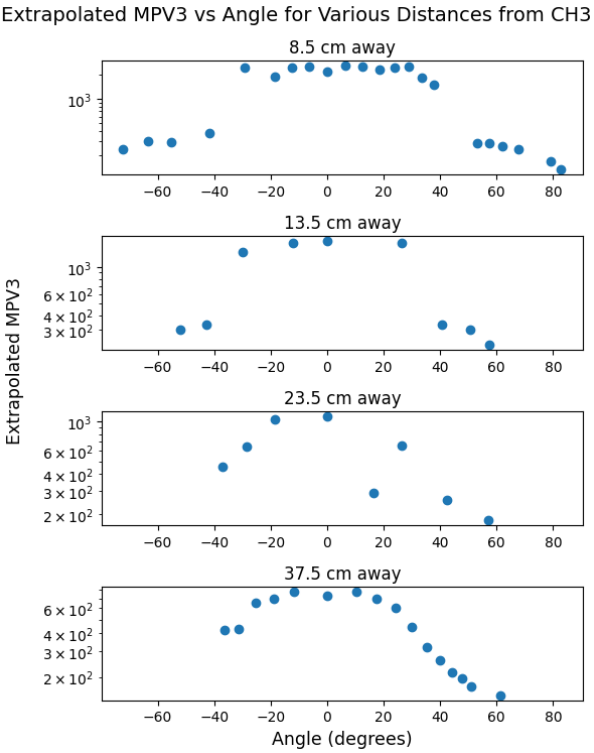

FIG. 9. A series of plots coordinating with scans across the slab at different distances across the width of the slab from CH3.

IV. DEVELOPMENT OF SIMULATION

To develop this better understanding of the milliQan slab detector, we also used data in this experiment to assist in the development of a simulation for photon generation and travel through the slab detectors. This simulation was developed first in the geometry of our slab detector, including many known physical phenomena, and compared directly with our data to confirm whether or not it is an accurate representation of the physics involved. Once this accuracy is confirmed, the geometry of the simulation will then be adjusted to match the milliQan slab detector, where it will be directly compared with their data. That comparison will serve as a confirmation as to whether we correctly understand all of the effects at play in the detector.

This simulation is currently in development, and it is in a relatively simple state. Photons are generated at a single point within a 2D equivalent to our detector with a speed determined by the refractive index of the material

and random direction. These photons travel in small steps until they reach a wall of the slab, where they run a series of checks, namely for total internal reflection, to determine whether the particle is reflected or absorbed. Upon absorption we check whether the photon is in the PMT. If it is, the photon is counted.

Though there are a number of effects missing and the photon generation method is crude, the simulation is currently in a state where it should be consistent with the effects seen in the analysis of our real data. A simple confirmation is creating the same plots that we did with real data. In this case, however, the data point we are plotting is going to be just the number of photons that reached each PMT instead of MPV.

As we can see from our new map and this direct comparison, the simulation agrees with our understanding of position-based effects to a reasonable extent. We see similar reductions in light collection further away from the PMT and the cutoff angle is present. There are a few clear differences, however. When the simulation gets beyond the cutoff, the response goes all the way to 0, while the real data has some minimum response that we're seeing. For the comparison at 8.5 cm away, we can also question whether the simulation is actually matching the "top hat" behavior we're seeing in the real data. Despite these differences, though, the simulation seems to be modeling the dominant effect. This simple version shows us the main effect we were targeting and can very easily be upgraded to include factors necessary for better matching.

V. OUTLOOK

Together the information gathered through scans of select regions on our slab detector and the simulation have provided us with a unique ability to improve our understanding of position-based effects that should be present in the milliQan slab detector. We successfully identified some basic trends and a dominant feature of the photon propagation, and we were able to make a simulation that matches these trends at a fundamental level. Through further scans of our slab detector and upgrades to the simulation, we can deepen our understanding of effects we have already seen and find new ones.

Once this simulation is improved and matching our detector's data well, we can adjust the geometry of the simulation to match the milliQan slab detector and begin comparing directly there. We can then adjust and potentially add more factors to the simulation to optimize the match to real data. Since these factors in the simulation match real phenomena, we can use this to confirm our understanding of how the angle and positioning of particles traveling through the slabs affect the sensitivity of the detector.

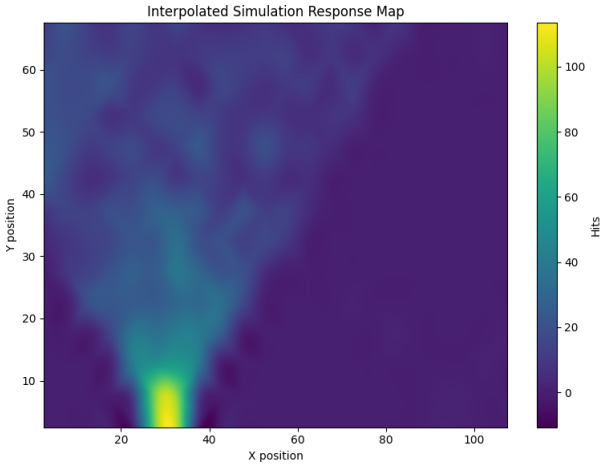

FIG. 10. A 2D histogram containing the simulated response. Note that the color scaling is no longer logarithmic.

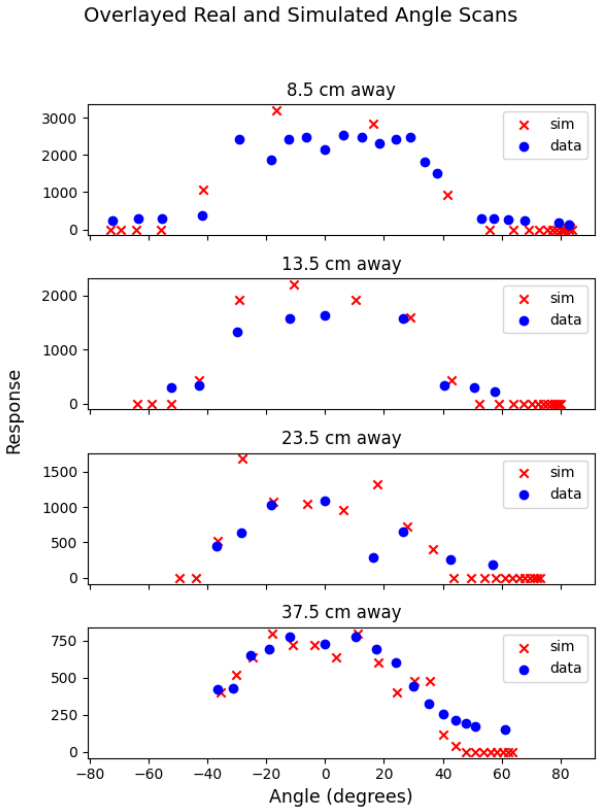

FIG. 11. A direct comparison of the measured CH3 angle scans and simulated scans in the same positions.

VI. ACKNOWLEDGMENTS

I would like to thank Prof. David Stuart for allowing me to work on this project and providing me with an opportunity to work in high-energy particle physics that I have not had up to this point. I'd also like to thank him for his mentorship over the course of the REU,

providing much-needed guidance and helping me refine my approach to analyzing and presenting research data.. Thank you to Dariush Imani and Eliott Schaffer as well for introducing me to the project, providing all the necessary information I needed to begin my research, and assisting me along the way. I would like to thank REU site director Prof. Sathya Guruswamy for allowing me to come to UCSB and participate in this REU and for making it an overall enjoyable experience. It is thanks to you all that I have gained much needed experience and an opportunity to learn about not just high-energy physics, but general skills I will need in future lab work. This work is supported by NSF REU grant PHY-2349677.

[1] J. H. Oort, The force exerted by the stellar system in the direction perpendicular to the galactic plane and some related problems, Bulletin of the Astronomical Institutes of the Netherlands **6**, 249 (1932), aDS Bibcode: 1932BAN.....6..249O.

[2] K. Garrett and G. Duda, Dark Matter: A Primer, Advances in Astronomy **2011**, 1 (2011), arXiv:1006.2483 [hep-ph].

[3] G. Jungman, M. Kamionkowski, and K. Griest, Supersymmetric dark matter, Physics Reports **267**, 195 (1996).

[4] F. Yu, enPrimer on Axion Physics, Annalen der Physik **536**, 2300106 (2024), _eprint: https://onlinelibrary.wiley.com/doi/pdf/10.1002/andp.202300106.

[5] X. C. 7, Dark Matter Search Results from a One Ton-Year Exposure of XENON1T, Physical Review Letters **121**, 111302 (2018), publisher: American Physical Society.

[6] P. W. Graham, I. G. Irastorza, S. K. Lamoreaux, A. Lindner, and K. A. v. Bibber, enExperimental Searches for the Axion and Axion-Like Particles, Annual Review of Nuclear and Particle Science **65**, 485 (2015), publisher: Annual Reviews.

[7] S. Gori, M. Williams, P. Ilten, N. Tran, G. Krnjaic, N. Toro, B. Batell, N. Blinov, C. Hearty, R. McGehee, P. Harris, P. Schuster, and J. Zupan, Dark Sector Physics at High-Intensity Experiments (2022), arXiv:2209.04671 [hep-ph].

[8] A. Berlin, J. A. Dror, X. Gan, and J. T. Ruderman, Millicharged Relics Reveal Massless Dark Photons, Journal of High Energy Physics **2023**, 10.1007/JHEP05(2023)046 (2023), arXiv:2211.05139 [hep-ph].

[9] S. e. a. Alcott, Search for millicharged particles in proton-proton collisions at $\sqrt{s} = 13.6$ TeV (2025), arXiv:2506.02251 [hep-ex].

[10] Hamamatsu Photonics, R878 Photomultiplier Tube (Head-on type), `https://www.hamamatsu.com/jp/en/product/optical-sensors/pmt/pmt_tube-alone/head-on-type/R878.html`, accessed: 2025-08-01.

[11] Eljen Technology, EJ-200, EJ-204, EJ-208, EJ-212 Plastic Scintillators, `https://eljentechnology.com/products/plastic-scintillators/ej-200-ej-204-ej-208-ej-212` (2021), accessed: 2025-08-01.

[12] R. D. Peccei and H. R. Quinn, CP Conservation in the Presence of Pseudoparticles, Physical Review Letters **38**, 1440 (1977), publisher: American Physical Society.

[13] e. a. Alexander, Dark Sectors 2016 Workshop: Community Report (2016), arXiv:1608.08632 [hep-ph].

[14] e. a. Battaglieri, US Cosmic Visions: New Ideas in Dark Matter 2017: Community Report (2017), arXiv:1707.04591 [hep-ph].

[15] L. Collaboration, Limits on Spin-Dependent WIMP-Nucleon Cross Section Obtained from the Complete LUX Exposure, Physical Review Letters **118**, 251302 (2017), publisher: American Physical Society.

[16] C. A. O'Hare, Can we overcome the neutrino floor at high masses?, Physical Review D **102**, 063024 (2020), publisher: American Physical Society.

[17] J. Billard, E. Figueroa-Feliciano, and L. Strigari, Implication of neutrino backgrounds on the reach of next generation dark matter direct detection experiments, Physical Review D **89**, 023524 (2014), publisher: American Physical Society.

[18] C. M. S. Collaboration, Dark sector searches with the CMS experiment, Physics Reports **1115**, 448 (2025), arXiv:2405.13778 [hep-ex].

[19] A. e. a. Ball, Search for millicharged particles in proton-proton collisions at $\sqrt{s}=13\text{ }\text{ }\mathrm{TeV}$, Physical Review D **102**, 032002 (2020), publisher: American Physical Society.